Scripta Materialia 113 (2016) 236–240

Contents lists available at ScienceDirect

Scripta Materialia

journal homepage: www.elsevier.com/locate/scriptamat

Regular Article

Microstructure and fracture toughness in boron added $NbSi_2$(C40)/$MoSi_2$($C11_b$) duplex crystals

Mitsuharu Todai [a], Koji Hagihara [b], Kyosuke Kishida [c,d], Haruyuki Inui [c,d], Takayoshi Nakano [a,*]

[a] Division of Materials and Manufacturing Science, Graduate School of Engineering, Osaka University, 2-1, Yamadaoka, Suita, Osaka 565-0871, Japan
[b] Department of Adaptive Machine Systems, Graduate School of Engineering, Osaka University, 2-1, Yamadaoka, Suita, Osaka 565-0871, Japan
[c] Department of Materials Science and Engineering, Kyoto University, Sakyo-ku, Kyoto 606-8501, Japan
[d] Center for Elements Strategy Initiative for Structural Materials (ESISM), Kyoto University, Sakyo-ku, Kyoto 606-8501, Japan

ARTICLE INFO

Article history:
Received 1 September 2015
Received in revised form 9 October 2015
Accepted 2 November 2015
Available online xxxx

Keywords:
Transition metal silicides
Lamellar structure
Toughness
Microstructure

ABSTRACT

The effect of B-addition on the microstructure and fracture toughness of $(Mo_{0.85}Nb_{0.15})Si_2$ crystals with an oriented lamellar microstructure was investigated. B-addition led to an increase in the volume fraction of the $C11_b$ phase, which possesses different orientation relationship from that of the fine lamellae, and a reduction in their precipitation rate. The fracture toughness of the B-added crystal with the varied microstructure exhibited a value more than 4.0 MPa $m^{1/2}$, that was significantly higher than that of the ternary crystal.

Transition metal disilicides, such as $MoSi_2$ with $C11_b$ structure and $NbSi_2$ with C40 structure are regarded as promising candidates for ultra-high-temperature structural materials because they have high melting points and good oxidation resistance. They can be expected to use at temperatures higher than the upper temperature limit of Ni-based superalloys [1–16]. However, these disilicides have some disadvantages which are low temperature brittleness and low creep resistance above 1473 K for industrial applications. To overcome these drawbacks, Nakano et al. developed a $NbSi_2$(C40)/$MoSi_2$($C11_b$) duplex crystal with an oriented fine lamellar microstructure [11]. This duplex crystal was obtained by the growth of the C40-structured $(Mo_{0.85}Nb_{0.15})Si_2$ single crystal and the following heat treatment at 1673 K. It was reported that this duplex crystal exhibits superior high temperature strength and enhanced low temperature fracture toughness [13,15]. The duplex crystals are comprised primarily of a fine C40/$C11_b$ lamellar microstructure, however, some $C11_b$ grains that do not have flat plate-like shapes are also formed when the C40-crystal is annealed at 1673 K for more than 24 h [11]. Those non-fine-lamellar-shaped $C11_b$ grains were found to rapidly grow and disarrange the oriented fine lamellae during prolonged (≥168 h) annealing. Thus, the control of the microstructure is essential to further improving the mechanical properties of the duplex crystal.

One approach for the microstructure control is the addition of another element to induce the segregation of these elements on the lamellar interface. Hagihara et al. [17,18] reported that the addition of some transition metals such as Cr and Zr led to significant improvement in the thermal stability of the oriented fine lamellar microstructure. However, the effect of adding non-transition elements to the duplex crystal remains unexplored. In the present study, we examine the effect of boron (B) additions on the formation of a lamellar microstructure and fracture toughness of the duplex crystal, because it is well known that the ductility and fracture mode of Ni-based alloys and TiAl are drastically improved by B-addition [19–21].

For our experiments, three master ingots having compositions of $(Mo_{0.85}Nb_{0.15})Si_2 - X$ at.% B ($X = 0$, 0.1 and 1.0) were prepared by arc melting of high-purity raw materials, such as Mo, Nb, Si and Mo_2B powder. Hereafter, the $(Mo_{0.85}Nb_{0.15})Si_2$ crystal is referred to as the ternary crystal and the B-added crystals are referred to by the percentage (X) of B added. Single crystalline rods with a C40 structure were grown by the floating zone (FZ) method at a rate of 2.5 mm/h under a high purity argon flow atmosphere. These rods were subsequently annealed at 1673 K for 24 h and 168 h in order to obtain an oriented lamellar microstructure composed of the C40 and $C11_b$ phases. The microstructures were observed by using an optical microscope and the crystal orientation relationship between the C40 matrix phase and the precipitated $C11_b$ phase was determined by the electron backscatter diffraction (EBSD) pattern analysis; EBSD date collection was conducted at a step size of 0.3 μm by using a scanning electron microscope (SEM, JEOL JEM-6500F).

The fracture toughness was examined by micro-Vickers hardness tests at room temperature at an applied load of 1000 gf. Indents were

* Corresponding author.
E-mail address: nakano@mat.eng.osaka-u.ac.jp (T. Nakano).

http://dx.doi.org/10.1016/j.scriptamat.2015.11.004
1359-6462/

made on the $(10\bar{1}0)$ plane of the C40 matrix phase. In addition, three-point bending tests were conducted at a cross-head speed of 0.005 mm min^{-1}, using an Instron-type testing machine. The fracture toughness value, K_Q based on the ASTM E399-90 guideline [22], was estimated by using the following equation:

$$K_Q = \left(F_Q S/BW^{3/2}\right) \times f(a/W) \quad (1)$$

where F_Q is the fracture load measured on the load–displacement line, and S, B, W and a donate the dimensions of the specimen, as shown in Fig. 4(b). The shape factor, indicated by $f(a/W)$, depends on the size of the specimen [22]. The loading axis was set to be parallel to the $[0001]_{C40}$; the lamellar boundary was laid perpendicular to the loading axis of the specimens. The notch being parallel to $(\bar{1}2\bar{1}0)_{C40}$ was introduced by using a diamond wire cutter.

Fig. 1 shows the variations in the microstructure with annealing period in the 0% (ternary), 0.1% and 1% B-added crystals. Fig. 1(a, d, g) shows the successful growth of C40-structured single crystals of each composition using the FZ method. The C40-single-phase microstructure in the ternary crystal evolved to oriented fine lamellae (Fig. 1(b)) with the precipitation of $C11_b$ phases by annealing at 1673 K for 24 h. However, a few $C11_b$ grains (indicated by the arrows) that do not have flat plate-like shapes formed in addition to the C40/$C11_b$ fine lamellae. The non-fine-lamellar-shaped $C11_b$ grains rapidly grew by further annealing to 168 h, resulting in the destruction of fine lamellar microstructure as shown in Fig. 1(c).

In contrast, the amount of $C11_b$ grains with non-flat interfaces increased significantly in the 0.1% and 1% B-added crystals (Fig. 1(e) and (h)) even by the annealing for 24 h. The volume fraction of non-fine-lamellar-shaped $C11_b$ grains were further increased by extending the annealing period to 168 h. It is to be noted that the size of those non-fine-lamellar-shaped $C11_b$ grains was kept to be smaller than that in the ternary crystal as shown in Fig. 1(f) and (i).

Fig. 2(a)–(f) exhibits the crystal orientation maps of the precipitated $C11_b$ phase in the annealed specimens, analyzed by SEM-EBSD method. The analyzed direction is parallel to the $[83\bar{1}\bar{1}0]_{C40}$, which is rotated by 15° from the $[10\bar{1}0]_{C40}$ to $[11\bar{2}0]_{C40}$ along the $[0001]_{C40}$ zone axis. The EBSD analysis and X-ray diffraction (XRD) measurements confirmed that all examined duplex crystals consisted of C40 and $C11_b$ phases; the black regions in Fig. 2(a)–(f) correspond to the C40 phase. In the ternary crystal, a large portion of the $C11_b$ grains exhibited a fine lamellar microstructure after 24 h annealing. Those grains were shown to belong to one of three colors; red, pink or purple, in Fig. 2(a). This is because these $C11_b$ phases had three orientation relationships with respect to the C40 matrix phase while maintaining the crystallographic relationship of $(0001)_{C40}//(110)_{C11b}$. The so-called strict-lamellar-variant orientation relationships denoted as variant 1 (V1), variant 2 (V2) and

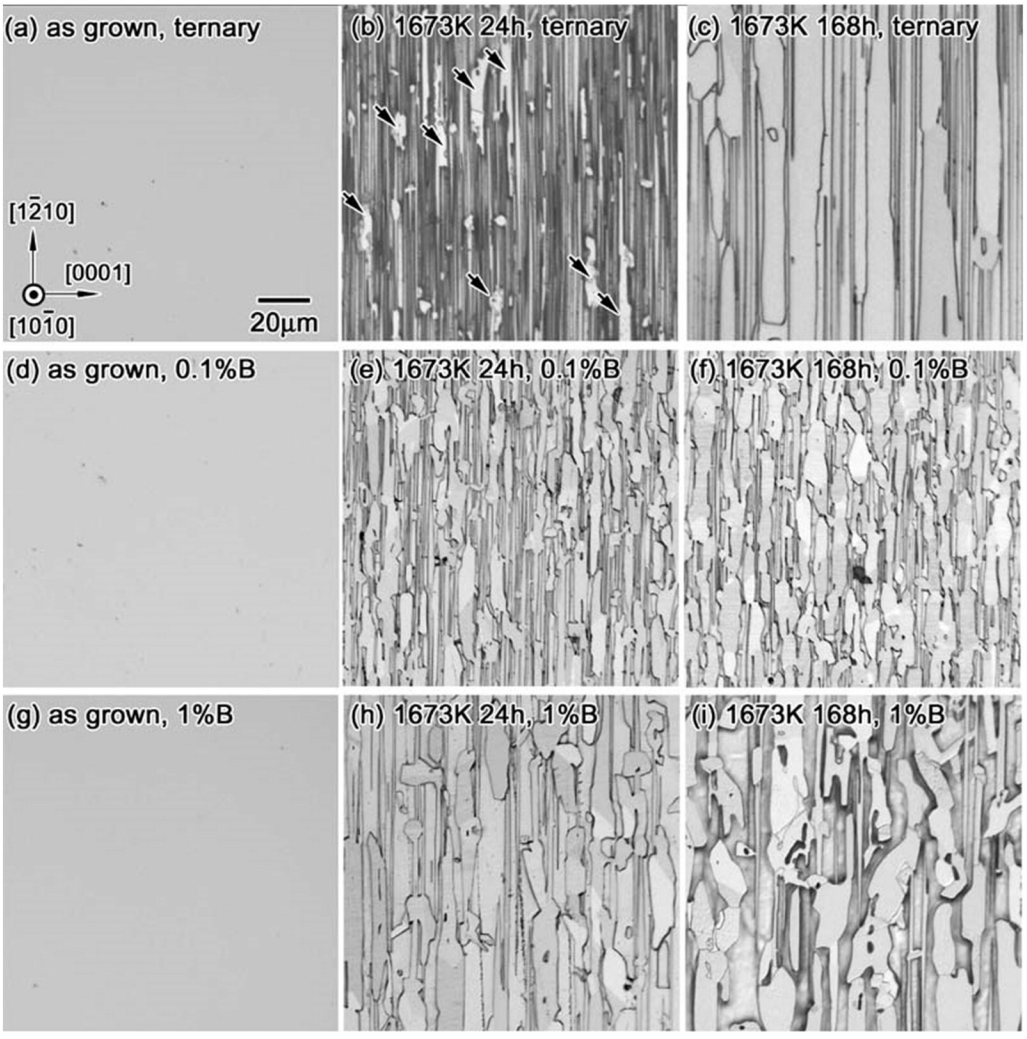

Fig. 1. Variations in the microstructure with annealing period in the (a–c) ternary, (d–f) 0.1% and (g–i) 1% B-added crystals. (a, d, g) as-FZ-grown, (b, e, h) annealed at 1673 K for 24 h, and (c, f, i) annealed at 1673 K for 168 h. The arrows in (b) show the non-fine-lamellar-shaped $C11_b$ phase.

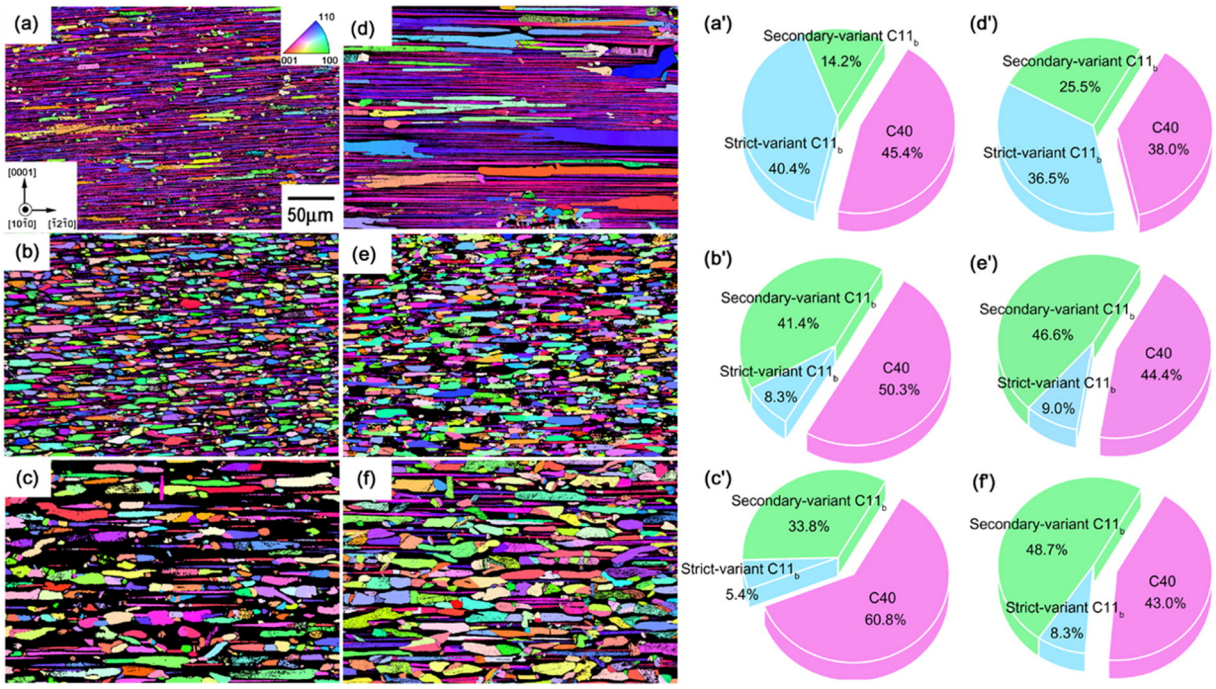

Fig. 2. Crystal orientation maps of the precipitated $C11_b$ phases in the C40 matrix examined by SEM-EBSD analysis, of specimens annealed at 1673 K for (a–c) 24 h and (d–f) 168 h, in the (a, d) ternary, (b, e) 0.1% and (c, f) 1% B-added crystals. The direction of observation in the microstructures was approximately parallel to the $[10\bar{1}0]_{C40}$, but the corresponding crystal orientation maps were colored along a direction rotated by 15° from the $[10\bar{1}0]_{C40}$ toward the $[11\bar{2}0]_{C40}$ to divide color of the three strict-lamellar-variants [17]. Pie charts (a′)-(f′) show the volume fractions of the C40 and $C11_b$ phases with strict-lamellar-variant orientation and secondary-variant orientation relationships in (a)–(f), respectively.

variant 3 (V3) were observed between the C40 phase and $C11_b$ phases as follows:

$$\mathrm{V1}: (0001)_{C40}//(110)_{C11b},\ [\bar{1}2\bar{1}0]_{C40}//[1\bar{1}0]_{C11b}, [10\bar{1}0]_{C40}//[001]_{C11b} \quad (2)$$

$$\mathrm{V2}: (0001)_{C40}//(110)_{C11b},\ [2\bar{1}\bar{1}0]_{C40}//[1\bar{1}0]_{C11b}, [0\bar{1}10]_{C40}//[001]_{C11b} \quad (3)$$

$$\mathrm{V3}: (0001)_{C40}//(110)_{C11b},\ [\bar{1}\bar{1}20]_{C40}//[1\bar{1}0]_{C11b},\ [\bar{1}100]_{C40}//[001]_{C11b} \quad (4)$$

As increasing in the annealing period, however, the volume fraction of fine $C11_b$ lamellae showing the above strict-lamellar-variant orientation relationships was decreased from 40.4% to 36.5%, owing to the rapid growth of the non-fine-lamellar-shaped $C11_b$ grains as shown in Fig. 2(d) and (d′).

As described in Fig. 1, B-addition was found to drastically reduce the volume fraction of the fine lamellar microstructure, and instead the amount of non-fine-lamellar-shaped $C11_b$ grains was increased, although the sizes were kept to be smaller than those in ternary crystal. SEM-EBSD analysis revealed that the non-fine-lamellar-shaped $C11_b$ grains were not randomly oriented, but a large fraction of them exhibited a certain crystal orientation relationship with respect to the C40 matrix phase. This relationship differs from the above-mentioned strict-lamellar-variant orientation relationship and is given as follows;

$$(0001)\langle 10\bar{1}0\rangle_{C40}//\{001\}\langle 010\rangle_{C11b} \quad (5)$$

$$(0001)\langle 10\bar{1}0\rangle_{C40}//\{001\}\langle 110\rangle_{C11b} \quad (6)$$

$$(0001)\langle 10\bar{1}0\rangle_{C40}//\{001\}\langle 210\rangle_{C11b} \quad (7)$$

$$(0001)\langle 10\bar{1}0\rangle_{C40}//\{111\}\langle 1\bar{1}0\rangle_{C11b} \quad (8)$$

$$(0001)\langle 10\bar{1}0\rangle_{C40}//\{12X\}\langle 2\bar{1}0\rangle_{C11b}. \quad (9)$$

These orientation relationships are similar to those observed in the non-fine-lamellar-shaped $C11_b$ grains in the ternary crystal [11, 17]. Hereafter, we refer to these orientation relationships as the secondary-variant orientation relationships. The composition of those constituent phases were examined by energy dispersive X-ray spectroscopy in the SEM (SEM-EDS), and it was confirmed that there is no significant variation in phase composition between the strict-variant $C11_b$ and secondary-variant $C11_b$ phases.

TEM observation of B-added crystals revealed that the growth of non-fine-lamellar-shaped $C11_b$ grains (secondary-variant $C11_b$ phase grains) frequently occurred accompanied by the absorption of the C40/$C11_b$ and $C11_b$/$C11_b$ fine lamellar boundaries. This feature is very similar to that previously reported in non-B-added crystal [11]. This suggests that a driving force for nucleation and grain growth of the secondary-variant $C11_b$ phase grain is the reduction in accumulated internal crystal strain on the lamellar boundaries, although the detailed nucleation mechanism of the secondary-variant $C11_b$ phase is not well clarified yet.

The variations in the microstructure indicate that the B-addition altered the precipitation rate of the $C11_b$ phase. In fact, the total amount of precipitated $C11_b$ phase decreased with increasing amount of B in the 24 h annealed crystals as shown in Fig. 2(a′)-(c′). Meanwhile, the amount of the $C11_b$ phase was about 60% in all specimens after annealing for 168 h as shown in Fig. 2(d′)-(f′). This suggests that the B-addition led to an increase in the incubation time for precipitation of the $C11_b$ phase and a decrease in the volume fraction of the $C11_b$ phases with strict-lamellar-variant orientation relationships.

Fig. 3 shows the variation in the average thickness of the fine-lamellar-shaped $C11_b$ grains with strict-lamellar-variant orientation relationships and the $C11_b$ grains with secondary-variant orientation relationships, measured along the $[0001]_{C40}$ direction on the $(10\bar{1}0)_{C40}$ in specimens annealed for 24 h and 168 h, respectively. The error bars in this figure correspond to the standard deviation of the thickness. As the figure shows, the average thickness of the $C11_b$ grains with the

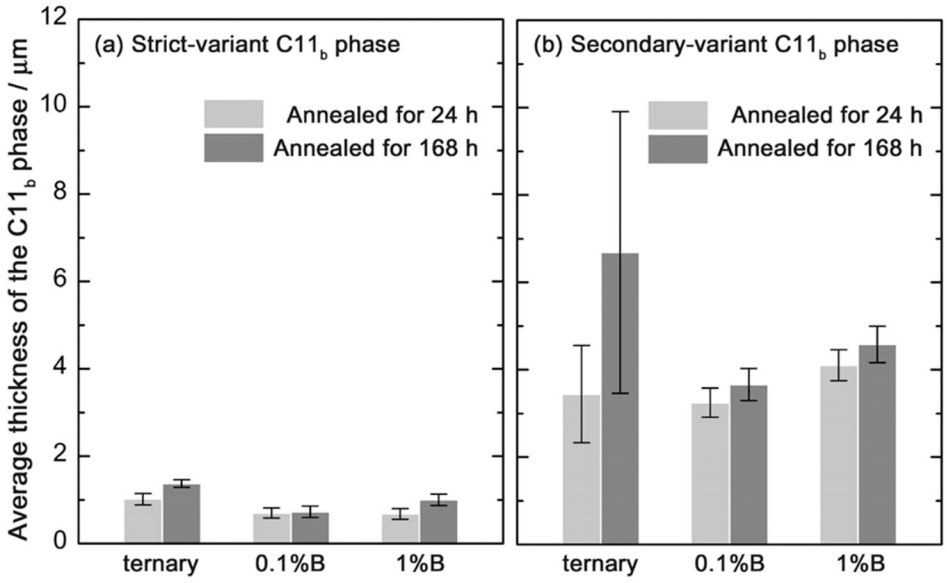

Fig. 3. Variation in the average lamellae thickness of the $C11_b$ grains with (a) strict-lamellar-variant and (b) secondary-variant orientation relationships in specimens annealed at 1673 K for 24 h and 168 h.

strict-lamellar-variant orientation relationships was almost the same independent of B-addition whereas the average thickness of the secondary-variant $C11_b$ grains changed significantly. The secondary-variant $C11_b$ grains in ternary crystals had average thickness of 3.4 and 6.7 μm after annealing for 24 h and 168 h, respectively. While those in the 0.1% and 1% B-added crystals were 3.2 and 4.1 μm after annealing for 24 h, and were as small as 3.7 and 4.5 μm after annealing for 168 h, respectively. These results demonstrate that the B-addition effectively suppresses the growth of the secondary-variant $C11_b$ grains.

It has been considered that the formation behavior of the lamellar microstructure is affected by the lattice misfit [17] and the interfacial energy [23] of the lamellar interface. According to Hagihara et al. [17], the thermal stability of the fine lamellar microstructure was improved and secondary-variant $C11_b$ grains almost disappeared by the reduced lattice misfit by Cr and Zr additions. On the other hand, phase-field simulations performed by Koizumi et al. revealed that a fine lamellar microstructure with flat interfaces on the $(0001)_{C40}$ does not form under conditions of isotropic interfacial energy [23]. In the present study, the B-addition led to a simultaneous increase in the volume fraction of the secondary-variant $C11_b$ grains and a decrease in the fraction of the fine-lamellar-shaped $C11_b$ grains. The B-addition may, therefore, lead to change in the interfacial energy rather than in the lattice misfit of the duplex crystals, although further studied are essentially required to validate this.

It is expected that significant refinement of the secondary-variant $C11_b$ grains has the potential to improve fracture toughness. In fact, grain size refinement led to substantial improvements in the room temperature fracture toughness of a $MoSi_2$ composite [24–26]. To confirm this, the indentation fracture toughness was first examined by using micro-Vickers hardness tests. This toughness, which is typically referred to K_{IC} was estimated by measuring the crack length (c) and micro-Vickers hardness (H) on the $(10\bar{1}0)_{C40}$ of the ternary, 0.1% and 1% B-added crystals [27]. The equation for estimating the K_{IC} classified for different crack systems. In this study, median-type cracks occurred in these crystals [13] and hence the value of K_{IC} was evaluated by the following equation [28,29],

$$K_{IC} = 0.016(E/H)^{1/2}\left(P/c^{3/2}\right) \quad (10)$$

where c is the median-type crack length, which is calculated from the observed crack length on the surface and half the diagonal of the indent. E is Young's modulus of the material along the indentation direction and P is the applied load (1000 gf in the case of this study). The E of the binary $NbSi_2$ single crystal [30] was used during the calculation of the K_{IC}, as rough estimations. Fig. 4(a) shows the variation in the estimated K_{IC} with annealing period. All the as-FZ-grown C40-structured single crystals exhibit a low K_{IC} of about 0.8–1.2 MPa $m^{1/2}$. The value of K_{IC} for ternary crystal increased upon annealing for 24 h, but decreased again by annealing for 168 h. This indicates that the development of a fine lamellar microstructure increases the fracture toughness K_{IC}, but the development of coarse secondary-variant $C11_b$ grains decreases the K_{IC}. Furthermore, B-added crystals had lower K_{IC} than that in the ternary crystal in 24 h annealed crystals. This must be owing to the decreases in volume fraction of the precipitated $C11_b$ phase in the B-added crystals compared to that in the ternary crystal by the reduction in the precipitation rate as described in Fig. 2. This highlights the importance of the $C11_b$ phase as a ductile phase. However, when the annealing period was extended to 168 h, B-added crystals have higher K_{IC} than the ternary crystal. This suggests that the suppression of the grain growth of secondary-variant $C11_b$ grains induced the suitable microstructure for increasing the fracture toughness.

We examined the variations in fracture toughness more precisely by performing three-point bending tests for 168 h annealed crystals, as the results are shown in Fig. 4(b). The 0.1% and 1% B-added crystals have average fracture toughness values of ~4.1 MPa $m^{1/2}$ and ~3.9 MPa $m^{1/2}$, respectively. These values are much higher than that (~2.8 MPa $m^{1/2}$) of the ternary crystal. This obviously demonstrates the validity of increase in fracture toughness by the suitable control of microstructure in duplex crystals.

In summary, we successfully controlled the microstructure of a $NbSi_2/MoSi_2$ duplex crystal by the B-addition. B-addition led to an increasing in the volume fraction of the $C11_b$ phase having secondary-variant orientation relationship, accompanied by the reduction in their growth rate. As a result, a microstructure composed of the C40 matrix phase, finer secondary-variant $C11_b$ grains, and strict C40/$C11_b$ fine lamellae was developed in the B-added crystal. It was found that this varied microstructure drastically improved the fracture toughness of the duplex crystal, exhibiting the highest value of ~4.5 MPa $m^{1/2}$ in the three-point bending test.

This work was supported by the "Advanced Low Carbon Technology Research and Development Program" of the Japan Science and

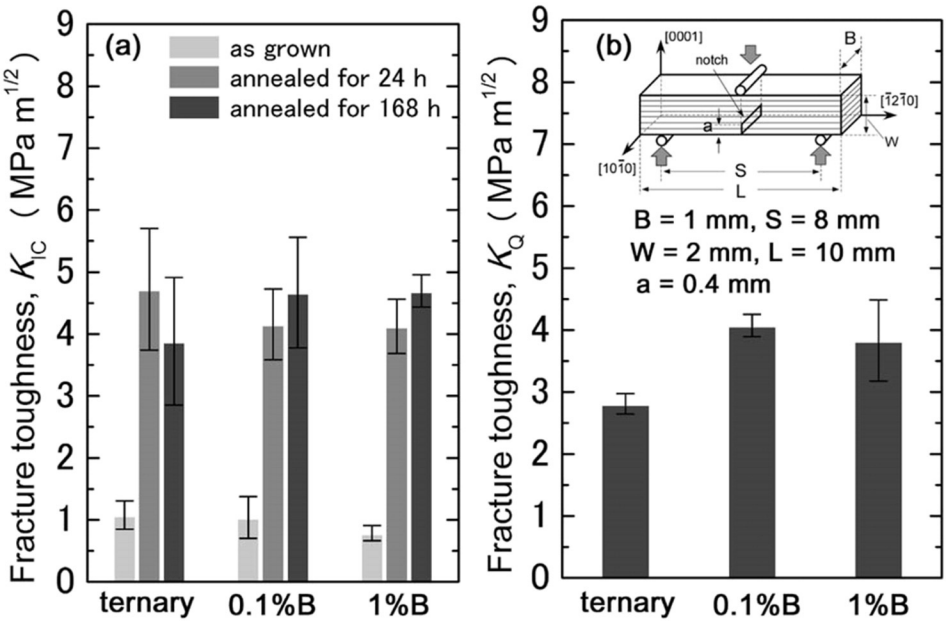

Fig. 4. (a) Indentation fracture toughness (K_{IC}) of the ternary, 0.1% and 1% B-added crystals with the C40 single-phase and C40/C11$_b$ duplex microstructures. (b) The fracture toughness values of the ternary, 0.1% and 1% B-added crystals annealed at 1673 K for 168 h evaluated by three-point bending tests.

Technology Agency and by the Grants-in-Aid for Scientific Research (S), No. 25220912 and Young Scientists (B), No. 26820315 from the Japan Society for Promotion of Science (JSPS). The authors are grateful to Mr. Kitani for his help with the experiments.

Appendix A. Supplementary data

Supplementary data to this article can be found online at http://dx.doi.org/10.1016/j.scriptamat.2015.11.004.

References

[1] A.K. Vasudevan, J.J. Petrovic, Mater. Sci. Eng. A 155 (1992) 1–17.
[2] Y. Umakoshi, T. Sakagami, T. Hirano, T. Yamane, Acta Metall. Mater. 38 (1990) 909–915.
[3] W.J. Boettinger, J.H. Perepezko, P.S. Frankwicz, Mater. Sci. Eng. A 155 (1992) 33–44.
[4] D.M. Shah, D. Berczik, D.L. Anto, R. Hecht, Mater. Sci. Eng. A 155 (1992) 45–57.
[5] K. Ito, H. Inui, Y. Shirai, M. Yamaguchi, Philos. Mag. A 72 (1995) 1075–1097.
[6] Y. Umakoshi, T. Nakano, E. Yanagisawa, T. Takezoe, A. Negishi, Mater. Sci. Eng. A 239-240 (1997) 102–108.
[7] T. Nakano, M. Azuma, Y. Umakoshi, Intermetallics 6 (1998) 715–722.
[8] K. Hagihara, T. Nakano, Y. Umakoshi, Scr. Mater. 38 (1998) 471–476.
[9] H. Inui, K. Ishikawa, M. Yamaguchi, Intermetallics 8 (2000) 1131–1145.
[10] T. Nakano, M. Kishimoto, D. Furuta, Y. Umakoshi, Acta Mater. 48 (2000) 3465–3475.
[11] T. Nakano, Y. Nakai, S. Maeda, Y. Umakoshi, Acta Mater. 50 (2002) 1781–1795.
[12] T. Nakano, K. Hagihara, Y. Nakai, Y. Umakoshi, Intermetallics 14 (2006) 1345–1350.
[13] K. Hagihara, S. Maeda, T. Nakano, Y. Umakoshi, Sci. Technol. Adv. Mater. 5 (2004) 11–17.
[14] F.G. Wei, Y. Kimura, Y. Mishima, Intermetallics 9 (2001) 661–670.
[15] K. Hagihara, T. Nakano, Acta Mater. 59 (2011) 4168–4176.
[16] K. Hagihara, T. Fushiki, T. Nakano, Scr. Mater. 82 (2014) 53–56.
[17] K. Hagihara, Y. Hama, K. Yuge, T. Nakano, Acta Mater. 61 (2013) 3432–3444.
[18] T. Yamazaki, Y. Koizumi, K. Yuge, A. Chiba, K. Hagihara, T. Nakano, K. Kishida, H. Inui, Intermetallics 54 (2014) 232–241.
[19] K. Aoki, O. Izumi, J. Jpn. Inst. Metals 43 (1979) 1190–1196.
[20] C.T. Liu, C.L. White, J.A. Horton, Acta Metall. 33 (1985) 213–229.
[21] T. Nakano, Y. Umakoshi, Intermetallics 2 (1994) 185–191.
[22] Annual book of ASTM Standards, E399-90, Standard test method for plane-strain fracture toughness of metallic materials, 1997.
[23] T. Yamasaki, Y. Koizumi, K. Yuge, A. Chiba, K. Hagihara, T. Nakano, K. Kishida, H. Inui, Comput. Mater. Sci. 108 (2015) 358–366.
[24] D.-K. Kim, I.-J. Shon, I.-Y. Ko, J.-K. Yoon, Z.A. Munir, Mater. Sci. Eng. A 457 (2007) 368–372.
[25] M. Patel, J. Subramanyuam, V.V.B. Prasad, Scr. Mater. 58 (2008) 211–214.
[26] J. Yan, H. Zhang, S. Tang, J. Xu, Mater. Charact. 60 (2009) 447–450.
[27] Y.K. Song, R.A. Varin, Intermetallics 6 (1998) 379–393.
[28] G.R. Anstis, P. Chantikul, B.R. Lawn, D.B. Marshall, J. Am. Ceram. Soc. 64 (1981) 533–538.
[29] P. Peralta, S.A. Maloy, F. Chu, J.J. Petrovic, T.E. Mitchell, Scr. Mater. 37 (1997) 1599–1604.
[30] F. Chu, M. Lei, S.A. Maloy, J.J. Petrovic, T.E. Mitchell, Acta Mater. 44 (1996) 3035–3048.